Sustainable Food Technology

ROYAL SOCIETY OF CHEMISTRY

PAPER

View Article Online
View Journal | View Issue

Cite this: *Sustainable Food Technol.*, 2025, **3**, 1151

Utilizing spent coffee grounds as sustainable fillers in biopolymer composites: influence of particle size and content†

Gabriel Mäder, Nadine Rüegg, Tobias Tschichold and Selçuk Yildirim *

This study presents the first systematic investigation of spent coffee grounds (SCG) particle size effects in polybutylene succinate (PBS) and polybutylene adipate terephthalate (PBAT) biocomposites, evaluating their potential as sustainable fillers in biodegradable polymers. Composites containing 30–60 wt% SCG were produced using unfractionated (SCG_m), coarse (SCG_L), and fine (SCG_S) particle size fractions. Thermogravimetric analysis (TGA) confirmed that both PBS and PBAT composites retained thermal stability up to processing temperatures of 220 °C, with onset degradation temperatures ranging from 266 °C to 294 °C for PBS and from 267 °C to 294 °C for PBAT. DSC analysis for PBS revealed an increase in glass transition temperature from −29.83 °C (neat) to −13.48 °C (60% SCG_m), while crystallinity remained stable (26.38–28.64%). Mechanical testing showed that SCG_m increased stiffness in both matrices. Young's modulus rose from 675 MPa (PBS) and 52 MPa (PBAT) up to 1016 MPa and 210 MPa, respectively. However, tensile strength declined from 34.5 MPa to 9.0 MPa (PBS) and from 18.8 MPa to 4.3 MPa (PBAT), and elongation at break dropped sharply, particularly in PBS (148% to 2.7%) and to a lesser extent in PBAT (446% to 12.4%). Finer SCG particles (SCG_S) enhanced ductility and water uptake (up to 3.40% for PBS and 4.42% for PBAT), while coarser particles (SCG_L) provided higher stiffness. Water contact angle and colour changes were minor across all samples. These results demonstrate that SCG can partially replace virgin biopolymer content in PBS and PBAT, enabling property tuning through particle size and promoting material circularity.

Received 7th May 2025
Accepted 2nd June 2025

DOI: 10.1039/d5fb00187k

rsc.li/susfoodtech

Sustainability spotlight

The production of bioplastics such as PBS and PBAT requires significant material and energy resources. This study addresses the challenge by partially replacing biodegradable polymers with coffee grounds (SCG), an abundant by-product of the food industry. Using SCG as a filler reduces virgin polymer consumption, enhances resource efficiency, and valorises food industry waste. The strategy supports a circular materials economy and aligns with the United Nations Sustainable Development Goals, specifically SDG 12 (Responsible Consumption and Production) and SDG 13 (Climate Action), by promoting resource efficiency, waste reuse, and the development of more sustainable materials for packaging and related applications.

1 Introduction

Plastics are ubiquitous in modern life due to their superior mechanical, thermal, and chemical properties, combined with low cost and ease of manufacturing.[1] Over the past decades, the use of plastics has increased exponentially, driven by demand across a wide range of industries including packaging, automotive, construction, and healthcare.[2] However, this rapid growth has led to significant environmental challenges, including heavy dependence on fossil resources,[3] contribution to climate change through greenhouse gas emissions,[3,4] and pervasive environmental pollution from non-biodegradable plastic waste.[4] These concerns have accelerated the development of alternative materials, particularly biobased and biodegradable polymers such as polylactic acid (PLA),[5,6] polybutylene succinate (PBS),[7–9] polybutylene adipate terephthalate (PBAT),[5,10] and polyhydroxyalkanoates (PHAs),[5,11] which are intended to replace conventional, fossil-based plastics. Despite these developments, the global market share of bioplastics remains very small compared to petroleum-based plastics.[12] A major limitation is that bioplastics often lack the mechanical and physical performance required for many demanding applications, limiting their competitiveness.[5] Furthermore, their production costs are significantly higher, restricting their use[13] especially for low-cost, high-volume applications such as

Zurich University of Applied Sciences, Department of Life Sciences and Facility Management, Campus Reidbach, 8820 Waedenswil, Switzerland. E-mail: selcuk.yildirim@zhaw.ch

† Electronic supplementary information (ESI) available. See DOI: https://doi.org/10.1039/d5fb00187k

food packaging. Addressing these challenges is critical for the broader adoption of bioplastics.[14]

At the same time, the food processing industry generates vast amounts of agricultural and industrial side streams, such as wheat bran, spent grain, barley rootlets, rapeseed press cake, whey, grape pomace, sugar beet pulp, date fruit pomace, coffee silver skin, spent coffee grounds, and cocoa bean husks.[15–26] Among these, spent coffee grounds (SCG), a byproduct of the coffee brewing process, have attracted considerable attention as a versatile and sustainable material. SCG has been investigated for diverse applications including building materials, bio-based pesticides, and photothermal systems for solar-driven water purification.[27–32] In the context of polymer science, SCG's lignocellulosic composition, rich in cellulose, hemicellulose, lignin, proteins, and lipids, makes it a promising candidate for enhancing the performance and sustainability of biopolymer composites.[15,17,33] Cellulose and hemicellulose can enhance stiffness and mechanical strength through fiber reinforcement, while lignin can improve thermal stability due to its aromatic structure.[34–36] Proteins may contribute to better interfacial adhesion with the polymer matrix, thus improving mechanical integrity.[37] Lipids and sugars can influence flexibility and impact resistance, and they can also affect the hydrophobicity of the material.[38,39]

Previous studies have demonstrated the integration of SCG into various biopolymers such as polylactic acid (PLA),[40] PLA/polyhydroxybutyrate (PHA) blends,[41] polybutylene succinate (PBS),[42,43] and polybutylene adipate terephthalate (PBAT),[44,45] with varying effects on the physical, mechanical, and thermal properties of the resulting composites. For instance, Bomfim *et al.* found that incorporating 10–30 wt% SCG into PLA modified crystallinity, reduced glass transition temperature, and increased toughness at moderate filler levels, although higher contents led to increased porosity and reduced density.[40] Gaidukova *et al.* reported that adding 20–60 wt% SCG to PBS increased stiffness and microhardness, but reduced tensile strength and elongation at break as the filler content rose. Thermal stability declined with higher SCG loading, while crystallinity remained consistently high (≥60%).[42] Similarly, Moustafa *et al.* observed that SCG incorporation in PBAT reduced tensile strength and ductility but improved stiffness, with the biocomposites showing good dispersion and increased surface hydrophilicity due to the presence of the hydrophilic lignocellulosic filler.[44] These studies emphasize that SCG can serve as a functional filler in bioplastics, yet also reveal that composite properties depend heavily on matrix type, filler loading, and interfacial compatibility.

Although only a few studies have investigated the incorporation of SCG into biopolymers, the influence of SCG particle size on the structure–property relationships of PBS and PBAT biocomposites remains insufficiently explored, limiting the optimization of their mechanical and physical performance. In this study, we address this gap by presenting the first systematic comparison of SCG particle size effects in PBS and PBAT matrices. We also extended the characterization of the resulting biocomposites, providing a more comprehensive understanding of how SCG content and particle size affect the thermal, mechanical, and physical properties of PBS and PBAT composites. Our objective was to evaluate the feasibility of utilizing SCG as a functional filler to enhance the performance of biopolymers, while providing more comprehensive material characterization to support the development of sustainable, cost-effective bioplastics for broader applications.

2 Materials and methods

2.1 Materials

Wet spent coffee grounds (SCG) were obtained from Emmi AG (Lucerne, Switzerland). PBS pellets (PBI 003, NaturePlast, Mondeville, France) with a density of 1.26 g cm^{-3} and a melt flow index (MFI) of 22 g/10 min (190 °C, 2.16 kg), as well as PBAT (biopolyester purge, BASF SE, Ludwigshafen, Germany) with a density of 1.25–1.29 g cm^{-3} and an MFI of 2.5–4.5 g/10 min (190 °C, 2.16 kg) were used in the composite formulations.

2.2 Milling and sieving of spent coffee grounds

Frozen SCG, stored at temperatures below −18 °C, were thawed at 4 °C for 24 h and subsequently pre-dried at 70 °C for 24 h in a climatic chamber (Binder GmbH, Tuttlingen, Germany). The dried material was then milled using a rotor impact mill (SR 300, Retsch GmbH, Haan, Germany) equipped with a 500 μm sieve insert and operated at 3000 rpm. Following grinding, the SCG powder was further dried at 70 °C and 1% relative humidity for 24 h, resulting in a final moisture content of 1.6%. The drying protocol (70 °C, 1% RH, 24 h) was selected to minimize residual moisture while preserving key bioactive compounds in SCG. Lower temperatures help avoid thermal degradation of sensitive components such as proteins and lipids, which can affect filler–matrix interactions, hydrophobicity, and composite colour. Particle size separation of the milled SCG was conducted using a vibratory sieve tower (AS 200 CA, Retsch GmbH, Haan, Germany) with mesh sizes of 500 μm, 400 μm, 300 μm, 200 μm, and 100 μm (compliant with ISO 3310-1), applying an amplitude of 1.2 mm. For subsequent investigations, the unsieved milled SCG (SCG_m) and fractions retained on the 400 μm sieve (SCG_L) and on the 200 μm sieve (SCG_S) were selected. The 200 μm and 400 μm cutoffs were chosen to obtain distinctly fine and coarse particle size fractions, allowing for a meaningful assessment of morphology-related effects on composite properties. The 200 μm threshold targets fine particles with high surface area and dispersion potential, while the 400 μm cutoff captures coarse particles expected to enhance stiffness due to their structural rigidity. These sizes were also guided by the observed particle distribution and practical considerations such as sufficient yield for processing and standard mesh availability in sieving equipment.

2.3 Particle size distribution and shape analysis

Particle size distribution and shape of the samples were analysed using a Camsizer X2 system (Retsch Technology, Germany), which operates based on the principle of dynamic image analysis in accordance with DIN EN ISO 13322-2:2021. The device covers a measurement range from 0.8 μm to 8 mm.

Approximately 12 g of SCG powder were introduced *via* a vibratory feeder. To ensure statistical significance, the minimum number of particles detected was set to 2 000 000 for the CCD-B camera and 2000 for the CCD-Z camera. Data acquisition and evaluation, including Q_3 and p_3 calculations, were performed using the instrument's control and analysis software (CamsizerX2).

2.4 Attenuated total reflection–fourier transform infrared spectroscopy (ATR–FTIR)

Infrared (IR) spectra of the SCG sample were recorded using a Spectrum Frontier spectrometer (PerkinElmer, USA) equipped with an attenuated total reflectance (ATR) unit. Each sample was scanned twenty times over a wavenumber range of 600–4000 cm^{-1} with a resolution of 4 cm^{-1}.

2.5 Compounding of biopolymer–spent coffee ground (SCG) composites

PBS and PBAT pellets were pre-dried at 60 °C for 10 hours before being blended with varying amounts of SCG_m (30 wt%, 40 wt%, 50 wt%, and 60 wt%) and two different particle size fractions (50 wt% SCG_L and 50 wt% SCG_S). The polymer–SCG mixtures were fed *via* a single-screw volumetric feeder and compounded using a co-rotating twin-screw extruder (ZE 18 HMI, ThreeTec, Switzerland), equipped with a double concave screw profile (screw diameter: 18 mm; L/D ratio: 25 : 1). For PBS-based blends containing 30 wt% or 40 wt% SCG, the screw speed was set to 30 rpm, while blends containing 50 wt% or more SCG were processed at 20 rpm. All PBAT-based formulations were extruded at 30 rpm. The temperature profile applied during compounding was 60/120/140/150/150 °C for both PBS and PBAT blends. The molten compound was shaped into a filament using a circular die (2 mm diameter), air-cooled under ambient conditions, and subsequently pelletized into approximately 3 mm-long pellets using a strand pelletizer (GRA ECO DN89-1 M, ThreeTec, Switzerland). The resulting pellets were then dried in a climate chamber (KWBF 720, Binder GmbH, Tuttlingen Germany) at 45 °C and 5% relative humidity for 24 hours.

2.6 Injection moulding of SCG-based specimens

Injection moulding was carried out using a laboratory-scale, custom-built injection moulding machine (S/N 21822, ThreeTec GmbH, Seon, Switzerland). The pellets were manually fed into the melt chamber, where the material was heated to 150 °C and held for 5 minutes prior to injection. The injection process was performed using an electrically driven piston, applying a pressure of 452 bar for 8 seconds, followed by a holding pressure of 283 bar for an additional 8 seconds. The mould temperature was maintained at 60 °C. Type 1BA dog bone test specimens were produced in accordance with ISO 527-2:2012, featuring a total length of ≥75 mm, a width of 5.0 ± 0.5 mm, and a thickness of ≥2.0 mm. The specimens were manually demoulded and subsequently conditioned in a climate chamber (VP600, Vötsch Industrietechnik, Balingen, Germany) at 23 ± 1 °C and 50 ± 5% relative humidity for at least 24 hours, following ISO 291:2008, prior to mechanical testing.

2.7 Thermogravimetric analysis (TGA)

Thermogravimetric analysis was performed on SCG, PBS, PBAT, and their respective compounds using a TGA 1 STARe System (Mettler-Toledo, Switzerland) coupled with a GC 200 STARe Gas Controller (Mettler-Toledo, Switzerland). Approximately 8 mg of each sample was placed in an alumina crucible, and measurements were conducted from 25 °C to 600 °C at a heating rate of 15 °C min^{-1} under a constant nitrogen flow of 40 ml min^{-1}.

2.8 Differential scanning calorimetry (DSC)

DSC analysis was conducted under a nitrogen atmosphere (50 ml min^{-1}) using a Q-2000 testing device (TA Instruments, USA). The tests were performed using 7 ± 1 mg of 100% PBS or PBS-SCG compounds. The samples were placed into an aluminium pan (TZero Pan & Hermetic Lid, TA Instruments, USA) and an empty pan was used as a reference. Prior to the measurements, the cup lids were punctured. The thermal program consisted of two heating–cooling cycles. Each cycle began with an isothermal hold at −90 °C for 5 minutes, followed by heating at a rate of 10 °C min^{-1} up to 250 °C. An isothermal hold at 250 °C was maintained for 1 minute before the sample was cooled back to −90 °C at a rate of −10 °C min^{-1}. Key thermal properties were obtained from the second heating cycle. The glass transition temperature (T_g) was determined as the inflection point corresponding to the temperature at which the slope of the step transition is steepest. The cold crystallization temperature (T_{cc}) and the melting temperature (T_m) were identified as the temperatures at the maxima of their respective exothermic and endothermic peaks. The enthalpy change associated with cold crystallization (ΔH_{cc}) was determined from the area under the exothermic peak, while the enthalpy of melting (ΔH_m) was calculated from the area under the endothermic peak. The degree of crystallinity (X_C) of PBS was calculated using eqn (1):

$$X_C = \left(\frac{\Delta H_m - \Delta H_{cc}}{f \cdot \Delta H_m^0}\right) \quad (1)$$

where ΔH_m is the melting enthalpy (J g^{-1}), ΔH_{cc} is the enthalpy of cold crystallization (J g^{-1}), f is the mass fraction of PBS in the composite, and $\Delta H_m{}^0$ is the melting enthalpy of 100% crystalline PBS, taken as 200 J g^{-1}.[46,47]

2.9 Tensile tests

The mechanical properties of the injection-moulded dog bone specimens were determined in accordance with ISO 527-1:2019 and ISO 527-2 using a universal testing machine (ProLine Z005 TH, ZwickRoell GmbH & Co. KG, Ulm, Germany), equipped with a 5 kN load cell and pneumatic grips rated up to 2.5 kN. The test speed was set to 1 mm min^{-1} for determination of the tensile modulus (E_t), and 50 mm min^{-1} for the determination of tensile strength (σ_m) and elongation at break (ε_b). Data acquisition and evaluation were carried out using testXpert III software (version

1.6). All values are reported as the mean ± standard deviation, based on eight replicate measurements per sample type.

2.10 Water uptake capacity (WUC)

Water uptake capacity (WUC) was determined for neat PBS, PBAT, and PBS–SCG compounds in accordance with DIN EN ISO 62:2008, using test specimens with a 1BA geometry as defined in ISO 527-2. Prior to testing, the samples were dried in a convection oven (FED 115, Binder, Germany) at 50 °C with 100% fan speed for 24 hours and weighed (m_1). Subsequently, the specimens were immersed in purified water (Arium Pro, Sartorius, Germany; conductivity: 0.055 μS cm^{-1}) for 24 hours, then removed and weighed again (m_2). Afterwards, the samples were re-dried under the same conditions (50 °C, 100% fan speed) for 96 hours and weighed a final time (m_3). Water uptake capacity was calculated as the relative mass change (c) as described in eqn (2). All measurements were performed in five replicates.

$$c = \frac{m_2 - m_3}{m_1} \quad (2)$$

2.11 Water contact angle (WCA)

The static water contact angle (WCA) of the injection-moulded specimen surfaces was determined using the sessile drop method with a goniometer (OCA15pro, DataPhysics Instruments GmbH, Filderstadt, Germany). The system was equipped with a 1 ml syringe (B. Braun, Germany) filled with ultrapure Milli-Q water and controlled *via* DataPhysics SCA20 software. A 10 μL droplet was dispensed onto the centre of the mould-side surface of each specimen at a feed rate of 1.05 μL s^{-1}. The contact angle of the droplet was calculated using the Young–Laplace fitting method implemented in the SCA20 software. For each material, five replicate measurements were performed using five different specimens.

2.12 Colour measurement

The colour of the test specimens was evaluated using a Chroma Meter (CR-410, Konica Minolta, Japan) based on the CIELAB colour space, which quantifies the L^*, a^*, and b^* parameters. Measurements were carried out on five specimens.

2.13 Statistical analysis

Results are reported as mean ± standard deviation. The data were tested for normal distribution using the Shapiro–Wilk test, and homogeneity of variances was assessed using Levene's test. If both assumptions were met, a one-way analysis of variance (ANOVA) was performed, followed by Tukey's HSD post-hoc test. In cases where at least one assumption was violated, the non-parametric Kruskal–Wallis test was used, followed by the Conover–Iman post-hoc test. Differences were considered statistically significant at $p < 0.05$. All statistical analyses were carried out using XLSTAT version 2023.2.1414 (Addinsoft, Paris, France). In all tables presenting group comparisons, statistically significant differences ($p \leq 0.05$) are indicated by different uppercase superscript letters, as determined by the appropriate post-hoc test.

3 Results and discussion

3.1 Characterization of spent coffee grounds (SCG) powders

3.1.1 Particle size distribution of SCG powders. Spent coffee grounds (SCG) were milled with an SR 300 rotor beater mill equipped with a 500 μm sieve and labelled as SCG_m. To investigate the influence of particle size on the material and physical properties of the compounds, the SCG_m was sieved through mesh sizes of 500, 400, 300, 200 and 100 μm. The powder retained on the 400 μm sieve was designated as SCG_L and the one retained on the 200 μm sieve as SCG_S. The particle size distribution (Q_3) and the density distribution (p_3) were determined for all three fractions, SCG_m, SCG_L, and SCG_S, as shown in Fig. 1. Both the unfractionated SCG_m and the sieved SCG_S exhibited a bimodal distribution in the cumulative distribution curves, indicating a heterogeneous particle size distribution with contributions from both fine and coarse fractions, which is also reflected in the two peaks of the density distributions. Despite selecting particles >200 μm for SCG_S, a notable proportion of smaller particles was present, likely due to the agglomeration of fine particles <200 μm adhering to larger ones during sieving. This is also supported by the observation that negligible material retained below the 200 μm sieve, even though a larger fine fraction would have been expected. In contrast, the SCG_L fraction exhibited a typical sigmoidal cumulative distribution, indicating a more uniform particle size distribution.

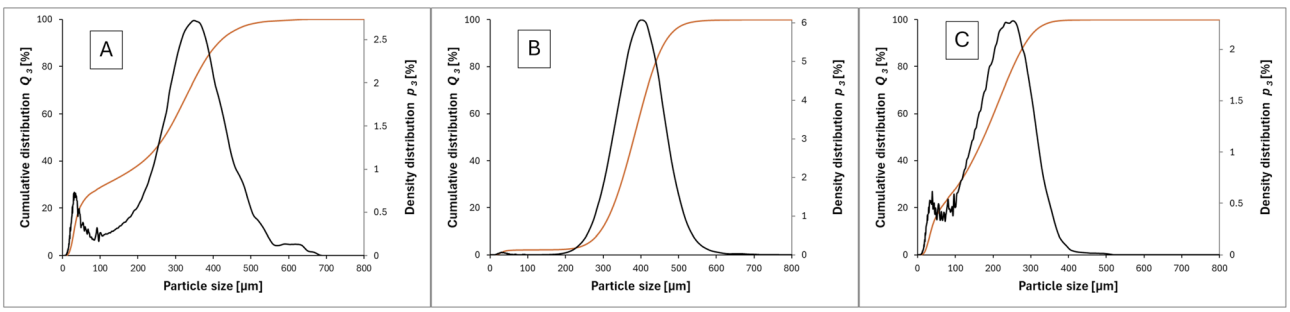

Fig. 1 Cumulative particle size distribution (Q_3) and density distribution (p_3) of spent coffee grounds (SCG) fractions. (A) Milled SCG with a 500 μm sieve insert (SCG_m); (B) sieved SCG with particle sizes between 400 and 500 μm (SCG_L); (C) sieved SCG with particle sizes between 200 and 300 μm (SCG_S).

Table 1 Key particle size and surface parameters of milled (SCG_m) and sieved spent coffee grounds (SCG_L and SCG_S). M_{v3}: volume-weighted mean diameter; S_v: specific surface area; $SPHT_3$: average shape factor; D_{32}: Sauter mean diameter

SCG-fraction	M_{v3} [μm]	S_v [mm^{-1}]	D_{32} [μm]	$SPHT_3$
SCG_m	236	63.6	121	0.778
SCG_L	375	18.7	381	0.901
SCG_S	168	61.7	125	0.778

The particle size distributions were further reflected in the volume-weighted mean diameter (M_{v3}) (Table 1). SCG_S fraction showed the lowest M_{v3} of 168 μm, indicating the predominance of small particles. The SCG_L exhibited the highest M_{v3} of 375 μm. The M_{v3} of the unfractionated powder SCG_m (236 μm) closely aligns with that of the fine fraction, rather than the coarse fraction, suggesting that fine particles are the dominant contributors to the volume distribution. The SCG_L fraction exhibited the lowest surface area-to-volume ratio (S_v = 18.7 mm^{-1}) and the highest Sauter diameter (381 μm), suggesting a lower surface area available for interfacial bonding with the biopolymer matrix compared to SCG_m and SCG_S. In contrast, SCG_m and SCG_S showed similar surface area-to-volume ratios (63.6 and 61.7 mm^{-1}, respectively) and Sauter diameters (121 and 125 μm), likely due to the dominant contribution of fine particles in both fractions. Furthermore, the average shape factors ($SPHT_3$) of SCG_m and SCG_S were identical at 0.778, indicating similarly irregular particle shapes. In comparison, SCG_L exhibited a higher shape factor (0.901), indicating a more spherical particle shape, which may contribute to the reduction of mechanical interlocking with the polymer matrix.

3.1.2 IR-spectroscopy (ATR-FTIR) of SCG. The FTIR spectrum of spent coffee grounds (SCG) shown in Fig. 2, reveals a broad and complex range of absorption bands corresponding to the material's heterogeneous biochemical composition. The broad band centered at 3336 cm^{-1} is attributed to O–H stretching vibrations from inter- and intramolecular hydrogen bonds, mainly associated with polysaccharides such as cellulose and hemicellulose, as well as phenolic hydroxyl groups in lignin.[48–51] A weak band at 3010 cm^{-1} is linked to C–H stretching in *cis*-configured double bonds (C=C), found in unsaturated fatty acids such as linoleic and oleic acids present in SCG.[52–56] The absorptions at 2923 cm^{-1} and 2854 cm^{-1} correspond to the stretching vibration of C–H bonds in aliphatic CH_2 groups, which are characteristic of fatty acid structures.[52,53] A well-defined absorption peak at 1744 cm^{-1} is characteristic of carbonyl C=O stretching vibrations from ester groups, typically associated with lipid components and other hydrocarbon-based structures.[33] The absorption at 1649 cm^{-1} is attributed to the C=C stretching vibration of *cis*-olefins (*cis*-RHC=CHR) and may also correspond to the C=O stretching vibration of amide I, characteristic of protein structures.[57–59] The absorption at 1456 cm^{-1} is associated with C–H bending vibrations in aliphatic CH_2 and CH_3 groups, whereas the band at 1377 cm^{-1} corresponds to symmetric C–H bending in CH_2 groups, typically attributed to coffee oil components.[52,54] The absorption band at 1240 cm^{-1} is linked to C–O–C linkages in cellulose and may also include C–O stretching vibrations from the O=C–O functional group in hemicelluloses.[60–62] The band at 1029 cm^{-1} arises from C–O and C–C stretching, and C6–H2–O6 vibrations, characteristic of cellulose structures.[63,64] Absorption at 808 cm^{-1} suggest the presence of chlorogenic acid isomers as well as C1–H bending in arabinans and arabinogalactans within the hemicellulose matrix.[63,65,66] The signal at 718 cm^{-1} results from overlapping aliphatic CH_2 rocking vibrations and out-of-plane deformations of *cis*-disubstituted olefins, commonly found in coffee oil components.[52,54] Overall, the FTIR data confirm the presence of multiple functional groups including hydroxyl, carbonyl, and ether linkages, which reflect the cellulose, hemicellulose, lignin, fat, and protein content of spent coffee grounds. It is important to note that the composition of SCG is subject to natural variability due to differences in coffee origin, bean type, roasting level, and brewing conditions. Such variability may affect the relative abundance of lignocellulosic and lipid components, potentially influencing filler–matrix interactions, thermal stability, and moisture uptake. While our study used a single, industrially sourced batch of SCG to ensure experimental consistency, future research may consider examining how the origin and processing of coffee influence composite performance and reproducibility.

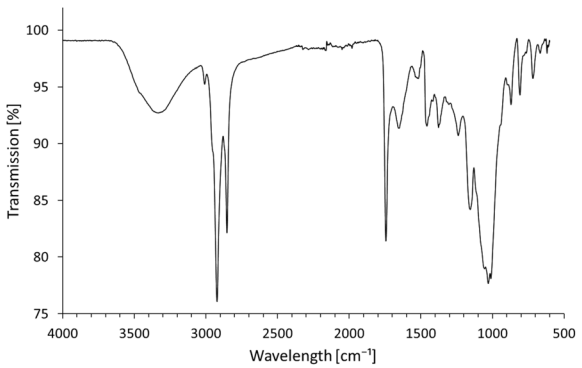

Fig. 2 ATR-FTIR spectra of dried spent coffee grounds (SCG).

3.1.3 Thermogravimetric analysis (TGA) of SCG. The thermal degradation behaviour of spent coffee grounds (SCG) was characterized using TGA and its derivative (DTG) under a nitrogen atmosphere (Fig. 3). Three distinct mass loss stages were observed. The first stage occurring below 150 °C, is attributed to the evaporation of physically adsorbed water and moisture loosely bound *via* hydrogen bonding.[67,68] The second stage, between approximately 200 °C and 350 °C, corresponds primarily to the decomposition of hemicelluloses and cellulose. A DTG peak at 307 °C indicates the maximum degradation rate of cellulose.[69] The third stage is characterized by a broad DTG peak with a shoulder around 330 °C and a maximum at 401 °C, reflecting the gradual thermal decomposition of lignin. Due to its complex aromatic structure, lignin degrades over a wide temperature range, extending to around 525 °C.[69,70] The thermal degradation of fatty acids, oils, and fats does not manifest as distinct DTG peaks but occurred over a broad temperature

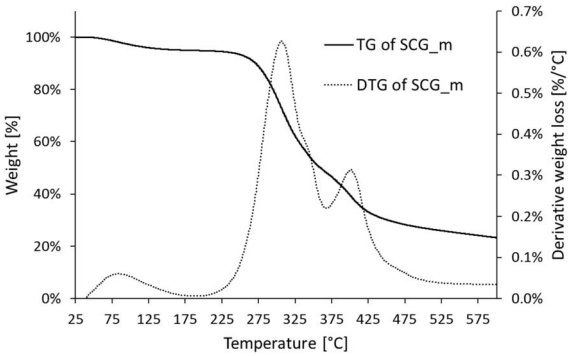

Fig. 3 TGA and DTG curve of dried and milled spent coffee grounds (SCG_m) recorded under nitrogen atmosphere using a heating rate of 15 °C min^{-1}.

range between 150 °C and 600 °C.[53,68] Overall, the TGA results confirm the typical multi-component thermal degradation behaviour of lignocellulosic biomass.

3.2 Influence of SCG loading on the thermal, mechanical and physical properties of PBS- and PBAT-based biocomposites

3.2.1 Thermogravimetric analysis (TGA) of PBS-SCG and PBAT-SCG compounds. Thermogravimetric analysis was used to evaluate the thermal stability of PBS and PBAT composites with varying SCG content (30–60 wt%). As shown in Fig. 4, all samples exhibited a characteristic three-stage mass loss profile. The first stage, occurring below 120 °C, represents the evaporation of residual moisture and physically adsorbed water. This effect was most pronounced in the sample containing only SCG_m, while it was negligible in the composite formulations, indicating effective drying during compounding and pelletizing. The second stage, observed between ~240 °C and 350 °C, corresponds to the thermal degradation of SCG components such as hemicellulose, cellulose, and partially lignin, along with minor contributions from lipids and other extractives. With increasing SCG content, mass loss in this region became more significant, reflecting the greater proportion of thermally labile biomass. The third stage occurred between ~350–425 °C for PBS-based composites and ~375–450 °C for PBAT-based composites. This phase is attributed to the decomposition of the polymer matrix and further degradation of lignin. For neat PBS, the onset degradation temperature was 364 °C with a DTG peak near 410 °C. In SCG–PBS composites, the onset temperature decreased as SCG content increased, ranging from 294 °C to 266 °C. Despite this shift, the DTG peaks remained stable around 400 °C, suggesting that the main degradation behavior of the PBS matrix remained unaffected. Gaidukova *et al.* observed a slightly lower DTG peak for neat PBS at 404 °C. In contrast to our results, the DGT peaks decreased more

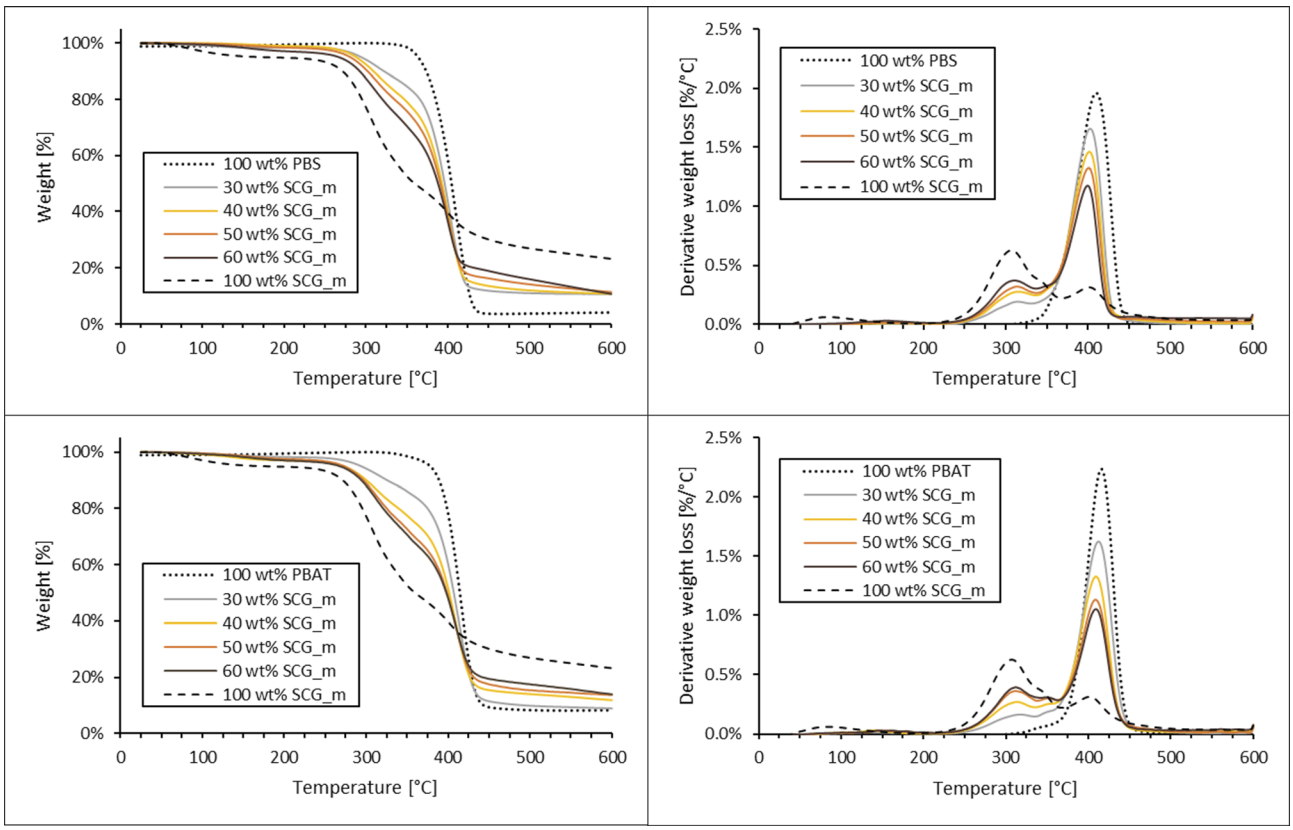

Fig. 4 TGA and DTG curves of neat PBS and PBAT, milled spent coffee ground (SCG_m) and their respective composites containing 30–60 wt% SCG. All measurements were conducted under constant nitrogen flow of 40 ml min^{-1} and a heating rate 15 °C min^{-1}.

significantly with the addition of SCG in their study, reaching 380 °C with 60 wt% SCG.[42] Similarly, neat PBAT degraded from an onset temperature of 378 °C with a DTG peak at ~416 °C. In SCG–PBAT composites, onset degradation temperatures dropped to the range of 294–267 °C with increasing SCG content, while DTG peaks remained unchanged. Comparable results were reported by Moustafa *et al.* who observed that the DTG peak of neat PBAT at 415 °C remained stable with the addition of 10–50 wt% SCG.[44] These findings indicate that the presence of SCG lowers the initial thermal stability of the composites due to the early decomposition of lignocellulosic material. However, the thermal integrity of both biopolymer matrices is largely preserved. This confirms that PBS and PBAT can be compounded with SCG at up to 60 wt% without critical impact on thermal behaviour, provided that processing temperatures remain below approximately 220 °C, a level safely below the onset of SCG degradation as determined by TGA.

3.2.2 Differential scanning analysis of PBS and PBS-SCG compounds. Differential Scanning Calorimetry (DSC) was performed to investigate the thermal transitions and crystallisation behaviour of neat PBS and PBS-SCG composites. The results shown in Table 2 were derived from the second heating cycle to eliminate thermal history effects. The incorporation of SCG_m into PBS lead to a clear increase in the glass transition temperature (T_g) rising from −29.83 °C in neat PBS to approximately −13 °C at 60 wt% SCG_m. This suggests a reduced mobility of the PBS polymer chains, likely caused by the rigid, fibrous structure of the SCG, which physically restricts chain movement.[43] In addition, polar functional groups present in SCG components, such as carbohydrates, may form intermolecular interactions, particularly hydrogen bonds, with PBS, further limiting chain flexibility. The distinct increase in T_g to −12.37 °C with SCG_m quantities of 40 w% and the fact that the value remains at around −13 °C with a further increase in SCG_m content indicates a saturation effect. The melting temperature (T_m) remained nearly constant (~114 °C) across all formulations, indicating that the crystalline phase of PBS was not significantly altered by the presence of SCG_m. However, the cold crystallization temperature (T_{cc}) increased with rising SCG_m content, while both the enthalpy of crystallization (ΔH_{cc}) and melting enthalpy (ΔH_m) decreased, consistent with partial suppression of crystal growth. This behavior likely results from steric hindrance caused by SCG particles, which interfere with chain alignment and reduce overall crystallization upon reheating. Despite these changes, the degree of crystallinity (X_c), when normalized to the PBS content, remained relatively stable (26–29%). This suggests that while SCG reduces the absolute crystallinity of the composite, PBS maintains its intrinsic ability to crystallize within its own phase. Overall, the results demonstrate that SCG incorporation modifies the thermal transition behavior of PBS, particularly by restricting chain mobility and nucleation during crystallization.

PBAT was not included in the DSC analysis due to its low degree of crystallinity and the presence of weak thermal transitions, which limit the suitability of this technique for detailed thermal characterisation.

3.2.3 Mechanical properties. The mechanical properties of PBS-based composites were significantly influenced by SCG content (Table 3). The Young's modulus increased from 675.2 ± 17.4 MPa for neat PBS to a maximum of 1015.8 ± 15.3 MPa at 40 wt% SCG_m, reflecting the stiffening effect of the rigid filler. However, at 50–60 wt% SCG_m, the modulus decreased slightly, likely due to matrix saturation and poor particle dispersion, which can lead to filler agglomeration and microvoid formation. Gaidukova *et al.* reported similar behaviour in PBS -SCG composites at comparable filler concentrations (0, 20, 40 and 60 wt%) noting a pronounced increase in brittleness beyond 40 wt% SCG. This was partly attributed to processing challenges during injection moulding.[42]

The tensile strength decreased continuously and significantly with increasing SCG content from 34.5 ± 2.0 MPa for neat PBS to 9.0 ± 0.1 MPa at 60 wt% SCG_m. This reduction is likely attributed to weak interfacial adhesion between the hydrophobic PBS matrix and the partially hydrophilic filler, leading to stress concentration and premature failure under tensile loading. While our interpretation of limited interfacial adhesion is based on mechanical performance trends and compositional considerations, we acknowledge that future studies could complement these findings with SEM analysis of fracture surfaces to directly assess filler–matrix bonding and dispersion. Gaidukova *et al.* observed the same effect in PBS/SCG composites with SCG proportions of 0–60%.[42] Elasticity decreased drastically from 148.1 ± 85.8% in neat PBS to 4.8 ± 0.5% already at an SCG_m content of 30 wt% and continued to decrease to 2.7 ± 0.1% at 60% SCG_m. This pronounced reduction in elongation at break highlights the embrittlement effect caused by the incorporation of SCG, which restricts polymer chain mobility and impairs the deformability of the PBS matrix. A

Table 2 Differential scanning calorimetry (DSC) data for neat PBS and PBS composites containing 30–60 wt% milled spent coffee grounds (SCG_m). Glass transition temperature (T_g), cold crystallisation temperature (T_{cc}), melting temperature (T_m), enthalpy of cold crystallisation (ΔH_{cc}), melting enthalpy (ΔH_m) and calculated crystallinity (X_c) are reported. All data were derived from the second heating cycle using, heating/cooling rates of 10 °C min^{-1}

PBS + SCG_m [wt%]	T_g [°C]	T_{cc} [°C]	T_m [°C]	ΔH_{cc} [J g^{-1}]	ΔH_m [J g^{-1}]	X_c [%]
0%	−29.83	96.65	114.09	9.78	62.54	26.38
30%	−27.42	99.70	113.97	6.33	44.63	27.36
40%	−12.37	101.32	113.64	4.43	36.30	26.56
50%	−13.09	103.36	113.52	2.26	28.82	26.56
60%	−13.48	104.04	113.63	1.09	24.00	28.64

Table 3 Young's modulus, tensile strength and elongation at break of injection-moulded dog-bone specimens made from PBS and PBAT and their composites containing 30–60 wt% milled spent coffee grounds (SCG_m). Values are expressed as mean ± standard deviation ($n = 8$). Different uppercase superscript letters within each column and polymer group (PBS or PBAT) indicate statistically significant differences between samples ($p \leq 0.05$)

Sample	Young's modulus [MPa]	Tensile strength [MPa]	Elongation at break [%]
PBS + SCG_m [wt%]			
0%	675.2 ± 17.4^{E}	34.5 ± 2.0^{A}	148.1 ± 85.8^{A}
30%	975.8 ± 19.9^{B}	17.7 ± 0.4^{B}	4.8 ± 0.5^{B}
40%	1015.8 ± 15.3^{A}	14.4 ± 0.1^{C}	4.0 ± 0.4^{C}
50%	916.5 ± 45.3^{C}	10.5 ± 0.3^{D}	2.8 ± 0.3^{D}
60%	877.2 ± 20.7^{D}	9.0 ± 0.1^{E}	2.7 ± 0.1^{D}
PBAT + SCG_m [wt%]			
0%	51.9 ± 5.0^{E}	18.8 ± 1.6^{A}	446.0 ± 53.4^{A}
30%	117.3 ± 11.9^{D}	8.8 ± 0.2^{B}	149.8 ± 14.8^{B}
40%	154.6 ± 12.9^{C}	6.5 ± 0.1^{C}	44.3 ± 9.4^{C}
50%	195.2 ± 15.4^{B}	5.1 ± 0.1^{D}	18.3 ± 2.9^{D}
60%	209.6 ± 18.0^{A}	4.3 ± 0.1^{E}	12.4 ± 1.9^{E}

similar trend, characterised by an increase in Young's modulus accompanied by a decrease in tensile strength and elongation, was observed in PBS composites containing 0–30% defatted SCG,[43] as well as in systems with SCG contents ranging from 0 to 60%.[42]

These mechanical trends in PBS–SCG_m composites align well with the thermal behavior observed in DSC analysis. The increase in glass transition temperature (T_g) with rising SCG content indicates reduced polymer chain mobility, which corresponds to the observed increase in stiffness (Young's modulus) and the pronounced decline in elongation at break. Although SCG reduced the overall crystallization enthalpies (ΔH_{cc} and ΔH_m), the degree of crystallinity (X_c) of PBS remained stable when normalized to its content, suggesting that the matrix retained its intrinsic crystallization potential, thus supporting mechanical rigidity.

PBAT-based composites exhibited similar trends but with some notable differences. The Young's modulus increased continuously with SCG content, reaching 209.6 ± 18.0 MPa at 60 wt% SCG_m, suggesting that even at higher loadings, the PBAT matrix retained sufficient continuity to transfer load. However, tensile strength and elongation at break decreased with increasing filler content, mirroring the PBS behavior. The initial elongation at break of PBAT (446.0 ± 53.4%) was significantly higher than that of PBS, reflecting its more ductile nature, but declined to 12.4 ± 1.9% at 60% SCG_m due to similar filler-induced embrittlement. The results obtained by Moustafa *et al.* show the same correlation for Young's modulus, tensile strength and elasticity at SCG concentrations between 0 and 50%.[44]

Overall, the results of the mechanical properties demonstrate that while SCG successfully stiffens both PBS and PBAT materials, however it reduces their tensile strength and flexibility due to reduced interfacial adhesion and increased brittleness.

3.2.4 Water uptake capacity, water contact angle and colour. Water absorption capacity (UC), water contact angle (WCA) and colour measurements of the manufactured materials were conducted on the injection-moulded dog bone specimen.

A consistent and significant increase in WUC was observed with increasing SCG_m content for both PBS and PBAT composites (Table 4). This can be attributed to both the hydrophilic nature of SCG components (*e.g.*, cellulose, hemicellulose, proteins) and the development of microvoids or microchannels at the filler–matrix interface. These microstructural defects increase the composite's porosity and create pathways for water ingress. PBAT composites exhibited slightly higher WUC values than PBS counterparts at equivalent SCG_m loadings, likely due to PBAT's greater flexibility and lower crystallinity, which may allow more moisture diffusion into the matrix.

The water contact angle (WCA) of neat PBS and PBAT was 87.44 ± 2.53° and 87.62 ± 2.01°, respectively. Incorporation of 30 wt% SCG_m significantly reduced the WCA to 80.72 ± 1.16° for PBS and 81.43 ± 0.90° for PBAT, indicating increased surface wettability. This initial decrease is likely due to the presence of hydrophilic functional groups from SCG components exposed at the composite surface. However, with further increases in SCG content, the WCA rose again, reaching 84.81 ± 1.07° for PBS and 89.30 ± 3.08° for PBAT at 60 wt% SCG_m. This reversal may be attributed to surface rearrangement during processing, where hydrophobic compounds such as lipids migrate toward the surface, forming a less polar outer layer and reducing overall surface wettability. A similar trend was observed by Alharbi *et al.* (2024) in PHBV/SCG composites at SCG loadings between 0% and 7%, attributing the initial reduction in WCA to the dominance of hydrophilic constitutes in SCG such as carbohydrates in SCG. They noted that both hydrophilic and hydrophobic components influence surface behaviour depending on their distribution. At higher filler concentrations, they suggested that surface film formation by oils and fats may account for the observed increase in contact angle.[71] In contrast, Moustafa *et al.* (2017) reported a continuous increase in WCA with increasing SCG content (0–30 wt%) highlighting the role of SCG drying conditions, particularly

Table 4 Water uptake capacity (WUC), water contact angle (WCA) and colour analysis ($L^*a^*b^*$) of injection molded dog bone specimens made from PBS, PBAT and their composites containing 30–60 wt% milled spent coffee grounds (SCG_m). Values are expressed as mean ± standard deviation ($n = 5$). Different uppercase superscript letters within each column and polymer group (PBS or PBAT) indicate statistically significant differences between samples ($p \leq 0.05$). * Statistical significance was determined based on full-resolution data prior to rounding

Sample	WUC [%]	WCA [°]	L^*	a^*	b^*
PBS + SCG_m [wt%]					
0%	0.38 ± 0.00^{A}	87.44 ± 2.53^{C}	81.7 ± 0.5^{A}	-1.6 ± 0.0^{C}	2.7 ± 0.1^{A}
30%	1.41 ± 0.03^{B}	80.72 ± 1.16^{A}	23.1 ± 0.5^{C}	1.2 ± 0.0^{A}	1.6 ± 0.1^{B}
40%	1.94 ± 0.02^{C}	80.70 ± 1.73^{A}	22.5 ± 0.5^{C}	1.0 ± 0.1^{B}	1.3 ± 0.1^{C}
50%	2.94 ± 0.06^{D}	83.35 ± 1.71^{B}	23.4 ± 0.3^{C}	1.1 ± 0.1^{B}	1.6 ± 0.1^{B}
60%	4.95 ± 0.09^{E}	84.81 ± 1.07^{BC}	25.3 ± 0.6^{B}	1.4 ± 0.2^{A}	2.8 ± 0.5^{A}
PBAT + SCG_m [wt%]					
0%	0.53 ± 0.01^{A}	87.62 ± 2.01^{C}	83.1 ± 0.9^{A}	-1.4 ± 0.1^{D}	3.1 ± 0.2^{A}
30%	2.42 ± 0.04^{B}	81.43 ± 0.90^{A}	23.7 ± 0.6^{B}	1.4 ± 0.1^{A}	2.1 ± 0.2^{B}
40%	3.00 ± 0.03^{C}	84.93 ± 1.58^{B}	23.6 ± 0.5^{B}	1.2 ± 0.1^{AB}	1.7 ± 0.1^{C}
50%	3.85 ± 0.10^{D}	87.84 ± 4.23^{BC}	23.7 ± 0.3^{B}	1.0 ± 0.1^{C} *	1.5 ± 0.1^{C}
60%	5.66 ± 0.12^{E}	89.30 ± 3.08^{C}	24.0 ± 0.3^{B}	1.0 ± 0.1^{BC} *	1.4 ± 0.2^{C}

temperature, in altering the material's surface chemistry and, consequently, its wettability.[44] In our case, the moderate drying temperature (70 °C) likely preserved a balanced profile of hydrophilic and hydrophobic constituents, which contributed to the initial reduction and later increase in water contact angle with higher SCG content.

Colour measurements revealed a substantial decrease in L^* values with SCG_m addition, reflecting reduced brightness due to the intrinsic dark brown coloration of SCG. However, L^* values stabilized beyond 30 wt% SCG_m, suggesting early saturation of colour intensity. Minor shifts in a^* and b^* values were observed, indicating slight red and blue tone changes, but these were not visually perceptible. The colour changes were largely consistent across both PBS and PBAT matrices, highlighting the dominant visual influence of the SCG filler (Fig. 5).

3.3 Influence of particle size of rapeseed press cake on the thermal, mechanical and physical characteristics of the compounds

3.3.1 Thermogravimetric analysis (TGA) of PBS-SCG and PBAT-SCG compounds containing different particle size of SCG. Thermogravimetric analysis was performed to assess the impact of spent coffee grounds (SCG) particle size on the thermal stability of PBS- and PBAT-based biocomposites. Biopolymers loaded with 50 wt% of SCG_m (unfractionated milled SCG), SCG_L (sieved SCG_m, obtained over the 400 μm sieve) or SCG_S (sieved SCG_m, obtained over the 200 μm sieve) were tested. The TGA and DTG curves of all composites, irrespective of particle size fraction, exhibited similar two-step degradation patterns, suggesting that filler particle size had no significant influence on the thermal degradation behaviour of the composites. All compounds experienced a first degradation step between 240 °C and 350 °C, which is attributed to the decomposition of SCG components such as hemicellulose, cellulose, fat, and partially lignin. A second stage of degradation occurred between ~350–425 °C in the PBS compounds and between ~375–450 °C in the PBAT compounds, mainly due to thermal decomposition of the polymer matrix and further decomposition of lignin components. The onset degradation temperatures of PBS composites were 281 °C (SCG_m), 274 °C (SCG_L), and 273 °C (SCG_S), while those for PBAT composites were 273 °C (SCG_m), 276 °C (SCG_L), and 268 °C (SCG_S). These minor differences confirm that particle size variation within the tested range does not critically affect the thermal stability of the composites. Therefore, all particle sizes can be considered thermally compatible with standard PBS and PBAT processing conditions.

Fig. 5 Injection-moulded dog-bone specimens made of neat PBS (A) or PBAT (B) and their respective composites containing 30, 40, 50 and 60 wt% milled spent coffee grounds (SCG_m).

3.3.2 Differential scanning analysis of PBS and PBS-SCG compounds. Differential Scanning Calorimetry (DSC) was conducted to evaluate the influence of SCG particle size on the thermal transitions and crystallization behaviour of PBS-based composites containing 50 wt% filler. All samples exhibited similar melting temperatures (T_m) ranging from 113.52 °C to 115.30 °C, indicating that the crystalline structure of PBS remained largely unaffected by SCG particle size. The cold crystallization temperature (T_{cc}) varied only slightly between samples, with values of 103.36 °C (SCG_m), 102.76 °C (SCG_L), and 105.42 °C (SCG_S), showing no systematic trend but reflecting minor differences in crystallization kinetics.

The melting enthalpy (ΔH_m) ranged from 28.82 J g^{-1} for SCG_m to 30.43 J g^{-1} for SCG_L, while the cold crystallization

enthalpy (ΔH_{cc}) varied from 1.71 J g^{-1} (SCG_S) to 4.09 J g^{-1} (SCG_L). Despite these small differences, the degree of crystallinity (X_c), normalized to the PBS content, remained relatively stable across all particle sizes: 26.56% (SCG_m), 26.34% (SCG_L), and 27.32% (SCG_S).

These results suggest that while SCG particle size has a limited effect on thermal transitions, finer particles (SCG_S and SCG_m) may slightly enhance crystallinity compared to coarser particles (SCG_L), possibly due to their higher surface area and better dispersion within the matrix, which can locally facilitate chain alignment. The glass transition temperature (T_g) varied slightly among the samples, with the highest T_g observed for SCG_L (−9.68 °C), followed by SCG_S (−10.68 °C), and the lowest T_g for the unfractionated SCG_m (−13.09 °C).

DSC analysis showed that SCG particle size had only a moderate effect on the thermal transitions of PBS composites. While melting and crystallization temperatures remained stable across all samples, minor variations in T_g and enthalpy values suggest subtle differences in chain mobility and crystallization behavior related to filler morphology and distribution.

3.3.3 Mechanical properties. The mechanical performance of PBS and PBAT composites was influenced not only by SCG content but also by the particle size and morphology of the filler. In PBS composites, the use of coarse SCG particles (SCG_L) resulted in the highest Young's modulus (1054.3 ± 22.1 MPa) (Table 5), which correlates with their larger volume-weighted mean diameter (Mv_3 = 375 μm), high Sauter diameter (381 μm), and low surface area-to-volume ratio (S_v = 18.7 mm^{-1}). This morphology likely promotes stiffness due to the rigid filler framework but limits interfacial area, resulting in the lowest elongation at break (2.5 ± 0.2%). Conversely, composites with SCG_S (finer particles, Mv_3 = 168 μm, D_{32} = 125 μm, S_v = 61.7 mm^{-1}) exhibited the highest elongation (4.1 ± 0.5%), likely due to increased filler dispersion and improved stress distribution. The unfractionated SCG_m (mixed particle sizes) showed intermediate mechanical properties and the lowest shape factor ($SPHT_3$ = 0.778), indicating more irregular particles that may increase mechanical interlocking and energy dissipation.

Similar trends were observed in PBAT composites, with SCG_S yielding the greatest elongation at break (26.7 ± 3.5%) and SCG_L showing reduced flexibility. The highest tensile strength and modulus in PBAT were recorded with SCG_m, suggesting that the mixed morphology offers a balance between rigidity and deformability. Overall, these results confirm that SCG particle size and shape directly influence filler–matrix interactions, affecting both stress transfer and composite ductility. Finer, irregular particles support better mechanical interlocking and flexibility, while coarse, spherical particles enhance stiffness at the expense of elongation.

3.3.4 Water uptake capacity, water contact angle and colour. Composites containing the finest SCG particles (SCG_S) exhibited the highest WUC for both polymer systems: 3.40 ± 0.06% in PBS and 4.42 ± 0.05% in PBAT (Table 6). This is consistent with the higher specific surface area and finer particle structure of SCG_S, which increases the exposure of hydrophilic groups (*e.g.*, cellulose, hemicellulose) and facilitates moisture absorption. In contrast, composites with coarser SCG particles (SCG_L) showed the lowest WUC values among the filled samples (2.87 ± 0.09% for PBS and 4.11 ± 0.10% for PBAT), likely due to reduced surface area and fewer accessible polar sites. SCG_m-based composites showed intermediate WUC values in both systems, reflecting the mixed nature of the particle distribution.

The WCA did not vary significantly among composites with different SCG particle sizes, remaining relatively stable within each polymer system. For PBS, values ranged narrowly between 82.07° and 83.85°, and for PBAT between 87.46° and 88.32°. These small differences suggest that particle size alone has a limited effect on surface wettability at the macroscopic scale, possibly because surface chemistry and processing-induced rearrangement of surface-active compounds (*e.g.*, lipids) play a more dominant role than morphology.

The PBS composites with small SCG particles (SCG_S) showed a significantly higher L^* value than the other two fractions suggesting that finer particles result in a slightly brighter surface, possibly due to better dispersion and more uniform light scattering. Meanwhile, a^* and b^* values remained

Table 5 Young's modulus, tensile strength and elongation at break of injection-moulded dog-bone specimens made from PBS, PBAT and their composites containing 50 wt% spent coffee grounds (SCG) with different particle sizes (SCG_m, SCG_L, SCG_S). Values are expressed as mean ± standard deviation (n = 8). Different uppercase superscript letters within each column and polymer group (PBS or PBAT) indicate statistically significant differences between samples ($p \leq 0.05$). Neat PBS and PBAT were not included in the statistical analysis

Sample	Young's modulus [MPa]	Tensile strength [MPa]	Elongation at break [%]
PBS + SCG [wt%]			
0% SCG	675.2 ± 17.4	34.5 ± 2.0	148.1 ± 85.8
50% SCG_m	916.5 ± 45.3^{B}	10.5 ± 0.3^{B}	2.8 ± 0.3^{B}
50% SCG_L	1054.3 ± 22.1^{A}	11.9 ± 0.4^{A}	2.5 ± 0.2^{A}
50% SCG_S	894.0 ± 40.3^{B}	10.9 ± 0.3^{B}	4.1 ± 0.5^{C}
PBAT + SCG [wt%]			
0% SCG	51.9 ± 5.0	18.8 ± 1.6	446.0 ± 53.4
50% SCG_m	195.2 ± 15.4^{A}	5.1 ± 0.1^{A}	18.3 ± 2.9^{B}
50% SCG_L	170.7 ± 16.6^{B}	5.0 ± 0.1^{B}	19.6 ± 3.2^{B}
50% SCG_S	148.3 ± 19.5^{C}	4.4 ± 0.1^{C}	26.7 ± 3.5^{A}

Table 6 Water uptake capacity (WUC), water contact angle (WCA) and colour analysis ($L^*a^*b^*$) of injection moulded dog-bone specimens produced of PBS and PBAT polymers and compounds of PBS or PBAT with spent coffee grounds (SCG) with different particle size (SCG, SCG_L, SCG_S). Values are expressed as mean ± standard deviation ($n = 5$). Different uppercase superscript letters within each column and polymer group (PBS or PBAT) indicate statistically significant differences between samples ($p \leq 0.05$). Neat PBS and PBAT were not included in the statistical analysis

Sample	WUC [%]	WCA [°]	L^*	a^*	b^*
PBS + SCG [wt%]					
0% SCG	0.38 ± 0.00	87.44 ± 2.53	81.7 ± 0.5	−1.6 ± 0.0	2.7 ± 0.1
50% SCG_m	2.94 ± 0.06^{A}	83.35 ± 1.71^{A}	23.4 ± 0.3^{B}	1.1 ± 0.1^{A}	1.6 ± 0.1^{B}
50% SCG_L	2.87 ± 0.09^{A}	82.07 ± 2.65^{A}	23.3 ± 0.3^{B}	1.0 ± 0.0^{A}	1.5 ± 0.1^{B}
50% SCG_S	3.40 ± 0.06^{B}	83.85 ± 2.53^{A}	26.1 ± 0.7^{A}	1.3 ± 0.3^{A}	2.6 ± 0.4^{A}
PBAT + SCG [wt%]					
0% SCG	0.53 ± 0.01	87.62 ± 2.01	83.1 ± 0.9	−1.4 ± 0.1	3.1 ± 0.2
50% SCG_m	3.85 ± 0.10^{A}	87.84 ± 4.23^{A}	23.7 ± 0.3^{B}	1.0 ± 0.1^{AB}	1.5 ± 0.1^{B}
50% SCG_L	4.11 ± 0.10^{B}	87.46 ± 3.14^{A}	24.8 ± 0.5^{A}	1.1 ± 0.1^{A}	1.8 ± 0.0^{A}
50% SCG_S	4.42 ± 0.05^{C}	88.32 ± 1.93^{A}	24.2 ± 0.3^{AB}	0.9 ± 0.0^{B}	1.3 ± 0.1^{C}

relatively stable, with only minor shifts indicating subtle changes in red-green and yellow-blue hues. In PBAT composites, these differences were less pronounced, and no significant trend was observed with changing in particle size.

These results confirm that SCG particle size primarily affects water uptake, with finer particles absorbing more moisture due to their higher surface area and exposure of hydrophilic sites. However, surface wettability (WCA) appears more dependent on surface chemistry and processing conditions than particle size. Visual brightness (L^*) is modestly enhanced by finer particles in PBS, but remains largely unaffected in PBAT, likely due to differences in polymer background colour and light reflection properties.

While this study thoroughly investigated the mechanical, thermal, and physical effects of incorporating spent coffee grounds (SCG) into PBS and PBAT composites, it is important to consider the biodegradation behavior of such materials to fully assess their environmental impact. Previous studies have demonstrated that both the type of biopolymer and the nature of the filler influence degradation kinetics. For example the addition of starch to PBAT-based films significantly accelerated biodegradation. Films with higher starch content, achieved complete degradation within 180 days, compared to minimal degradation in starch-free PBAT films.[72] Although biodegradation tests were not conducted in the current work, these findings suggest that the addition of SCG, particularly in fine particle sizes with higher surface areas, could impact microbial accessibility, water retention, and degradation kinetics. Therefore, future studies should incorporate controlled biodegradation analyses to elucidate how SCG particle size and concentration influence the environmental fate of these composites.

Conclusions

This study demonstrates the feasibility of incorporating spent coffee grounds (SCG) as a sustainable filler in PBS and PBAT biopolymer matrices, with a particular focus on the influence of filler content and particle size on composite performance. Thermogravimetric analysis confirmed that both PBS and PBAT can be compounded with up to 60 wt% SCG without critical degradation of thermal stability, provided processing temperatures remain below 220 °C. This underlines the importance of maintaining processing temperatures below 220 °C in industrial applications to ensure material integrity and prevent degradation of SCG components. DSC analysis revealed that SCG incorporation increased the glass transition temperature (T_g) and cold crystallization temperature (T_{cc}) of PBS, while the melting temperature (T_m) and normalized crystallinity (X_c) remained largely unaffected, indicating that PBS retains its intrinsic crystallization capacity even at high filler loadings. Mechanically, SCG acted as a reinforcing phase at moderate contents, increasing stiffness (Young's modulus) in both PBS and PBAT composites. However, tensile strength and elongation at break declined with increasing SCG content, attributed to poor interfacial adhesion and limited stress transfer efficiency. Mechanical test with different particle sizes showed that coarser SCG particles (SCG_L) enhanced stiffness but caused greater embrittlement, while finer particles (SCG_S) improved ductility and stress distribution due to better dispersion and higher interfacial area. The physical properties of the composites were also influenced by SCG particle size. Water uptake capacity increased with finer particles, reflecting their higher surface area and hydrophilic character. In contrast, water contact angle and colour parameters showed only minor dependence on particle size, with wettability more likely governed by surface chemistry and processing conditions. Overall, SCG represents a promising biofiller for enhancing the sustainability of biodegradable polymers, offering a means to reduce virgin polymer content and valorize agro-industrial waste. Optimizing particle size and filler content is critical to balancing mechanical performance, thermal stability, and moisture sensitivity in bioplastic formulations. Given their increased stiffness and reduced elongation, SCG–PBS composites may be suited for rigid packaging or disposable items where structural integrity is more critical than flexibility. Conversely, SCG–PBAT formulations with finer particles, which retained some ductility, could be considered for applications such as

biodegradable mulch films or flexible agricultural materials. These application pathways highlight the potential of SCG-filled biocomposites to be tailored for specific end-use scenarios depending on filler content and morphology. The elevated water uptake capacity observed in composites with higher SCG content may facilitate microbial colonization and hydrolytic degradation, potentially accelerating environmental breakdown under composting or soil conditions. Future studies should incorporate controlled biodegradation analyses to elucidate how SCG particle size and concentration influence the environmental fate of these composites.

Data availability

The data supporting this article have been included within the article and additionally as part of the ESI.†

Author contributions

Gabriel Mäder: conceptualization, methodology, investigation, visualization, project administration, writing – original draft. Nadine Rüegg: investigation. Tobias Tschichold: investigation. Selçuk Yildirim: conceptualization, funding acquisition, methodology, supervision, writing – original draft, writing – review and editing.

Conflicts of interest

There are no conflicts to declare.

Acknowledgements

We thank the Avina Foundation for providing funding.

References

1 L. Lebreton and A. Andrady, *Palgrave Commun.*, 2019, **5**, 6.
2 K. Houssini, J. Li and Q. Tan, *Commun. Earth Environ.*, 2025, **6**, 257.
3 J. P. Tilsted, F. Bauer, C. D. Birkbeck, J. Skovgaard and J. Rootzén, *One Earth*, 2023, **6**, 607.
4 M. Shen, W. Huang, M. Chen, B. Song, G. Zeng and Y. Zhang, *J. Cleaner Prod.*, 2020, **254**, 120138.
5 X. Zhao, K. Cornish and Y. Vodovotz, *Environ. Sci. Technol.*, 2020, **54**, 4712.
6 T. A. Swetha, A. Bora, K. Mohanrasu, P. Balaji, R. Raja, K. Ponnuchamy, G. Muthusamy and A. Arun, *Int. J. Biol. Macromol.*, 2023, **234**, 123715.
7 M. J. Mochane, S. I. Magagula, J. S. Sefadi and T. C. Mokhena, *Polymers*, 2021, **13**, 1200.
8 M. Barletta, C. Aversa, M. Ayyoob, A. Gisario, K. Hamad, M. Mehrpouya and H. Vahabi, *Prog. Polym. Sci.*, 2022, **132**, 101579.
9 O. Platnieks, S. Gaidukovs, V. K. Thakur, A. Barkane and S. Beluns, *Eur. Polym. J.*, 2021, **161**, 110855.
10 S. Roy, T. Ghosh, W. Zhang and J.-W. Rhim, *Food Chem.*, 2024, **437**, 137822.
11 J. C. C. Yeo, J. K. Muiruri, X. Fei, T. Wang, X. Zhang, Y. Xiao, W. Thitsartarn, H. Tanoto, C. He and Z. Li, *Biomater. Adv.*, 2024, **163**, 213929.
12 European Bioplastics, Bioplastic materials, **https://www.european-bioplastics.org/bioplastics/materials/**, accessed 28th April 2025.
13 C. Wellenreuther, A. Wolf and N. Zander, *Cleaner Eng. Technol.*, 2022, **6**, 100411.
14 M. Ghasemlou, C. J. Barrow and B. Adhikari, *Food Packag. Shelf Life*, 2024, **43**, 101279.
15 C.-T. Wu, D. C. Agrawal, W.-Y. Huang, H.-C. Hsu, S.-J. Yang, S.-L. Huang and Y.-S. Lin, *J. Chem.*, 2019, **2019**, 671438.
16 C. Kourmentza, C. N. Economou, P. Tsafrakidou and M. Kornaros, *J. Cleaner Prod.*, 2018, **172**, 980.
17 C. V. Garcia and Y.-T. Kim, *J. Polym. Environ.*, 2021, **29**, 2372.
18 A. Beldycka-Borawska, *Roczniki*, 2023, **2023**, 4.
19 E. Sirmacekic, A. Atilgan, R. Rolbiecki, B. Jagosz, S. Rolbiecki, O. Gokdogan, M. Niemiec and J. Kocięcka, *Energies*, 2022, **15**, 9636.
20 M. Ptak, A. Skowrońska, H. Pińkowska, M. Krzywonos, M. Ptak, A. Skowrońska, H. Pińkowska and M. Krzywonos, *Energies*, 2022, **15**, 175.
21 A. J. Garcia-Brand, M. A. Morales, A. S. Hozman, A. C. Ramirez, L. J. Cruz, A. Maranon, C. Muñoz-Camargo, J. C. Cruz and A. Porras, *Polymers*, 2021, **13**, 3707.
22 W. Cheng, Y. Sun, M. Fan, Y. Li, L. Wang and H. Qian, *Crit. Rev. Food Sci. Nutr.*, 2022, **64**, 6636.
23 M. Bordiga, F. Travaglia and M. Locatelli, *Int. J. Food Sci. Technol.*, 2019, **54**, 933.
24 L. Nyhan, A. W. Sahin, H. H. Schmitz, J. B. Siegel and E. K. Arendt, *J. Agric. Food Chem.*, 2023, **71**, 10543.
25 E. Neylon, E. K. Arendt, K. M. Lynch, E. Zannini, P. Bazzoli, T. Monin, A. W. Sahin, E. Neylon, E. K. Arendt, K. M. Lynch, E. Zannini, P. Bazzoli, T. Monin and A. W. Sahin, *Fermentation*, 2020, **6**, 117.
26 V. M. Rangaraj, K. Rambabu, F. Banat and V. Mittal, *Food Chem.*, 2021, **355**, 129631.
27 J. Shao, Z. Chen, S. Luo, S. Liu, X. Sun, H. Wen and L. Su, *Journal of Building Engineering*, 2024, **97**, 110910.
28 R. Roychand, S. Kilmartin-Lynch, M. Saberian, J. Li, G. Zhang and C. Q. Li, *J. Cleaner Prod.*, 2023, **419**, 138205.
29 F. G. Horgan, D. Floyd, E. A. Mundaca and E. Crisol-Martínez, *Agriculture*, 2023, **13**, 257.
30 P.-C. Hsieh, Y.-C. Chen, N.-C. Zheng, D. Mangindaan and H.-W. Chien, *J. Ind. Eng. Chem.*, 2023, **126**, 283.
31 C. Shi, X. Zhang, A. Nilghaz, Z. Wu, T. Wang, B. Zhu, G. Tang, B. Su and J. Tian, *Chem. Eng. J.*, 2023, **455**, 140361.
32 X. Luo, L. Zhou, R. Zheng, H. Zhang, B. Wang, Y. Mei and R. Chen, *ACS Appl. Mater. Interfaces*, 2023, **15**, 59973.
33 D. Pujol, C. Liu, J. Gominho, M. À. Olivella, N. Fiol, I. Villaescusa and H. Pereira, *Ind. Crops Prod.*, 2013, **50**, 423.
34 G. Siqueira, J. Bras, N. Follain, S. Belbekhouche, S. Marais and A. Dufresne, *Carbohydr. Polym.*, 2013, **54**, 711.
35 O. Platnieks, S. Gaidukovs, A. Barkane, A. Sereda, G. Gaidukova, L. Grase, V. K. Thakur, I. Filipova, V. Fridrihsone, M. Skute and M. Laka, *Polymers*, 2020, **12**, 1472.

36 M. R. Ridho, E. A. Agustiany, M. R. Dn, E. W. Madyaratri, M. Ghozali, W. K. Restu, F. Falah, M. A. R. Lubis, F. A. Syamani, Y. Nurhamiyah, S. Hidayati, A. Sohail, P. Karungamye, D. S. Nawawi, A. H. Iswanto, N. Othman, N. A. M. Aini, M. H. Hussin, K. Sahakaro, N. Hayeemasae, M. Q. Ali and W. Fatriasari, *Adv. Mater. Sci. Eng.*, 2022, **2022**, 363481.
37 E. Álvarez-Castillo, M. Felix, C. Bengoechea, A. Guerrero, E. Álvarez-Castillo, M. Felix, C. Bengoechea and A. Guerrero, *Foods*, 2021, **10**, 981.
38 J. A. Sirviö, M. Visanko, J. Ukkola and H. Liimatainen, *Ind. Crops Prod.*, 2018, **122**, 513.
39 T. T. Ngo, C. A. Lambert, M. Bliznyuk and J. G. Kohl, *Polym.-Plast. Technol. Eng.*, 2013, **52**, 1160.
40 A. S. C. de Bomfim, D. M. de Oliveira, K. Benini, M. O. H. Cioffi, H. J. C. Voorwald and D. Rodrigue, *Polymers*, 2023, **15**, 2719.
41 J. Y. Boey, U. Kong, C. K. Lee, G. K. Lim, C. W. Oo, C. K. Tan, C. Y. Ng, A. A. Azniwati and G. S. Tay, *Int. J. Biol. Macromol.*, 2024, **266**, 131079.
42 G. Gaidukova, O. Platnieks, A. Aunins, A. Barkane, C. Ingrao and S. Gaidukovs, *RSC Adv.*, 2021, **11**, 18580.
43 Y. Fang, Z. Jiang, X. Zhao, J. Dong, X. Li and Q. Zhang, *Compos. Commun.*, 2022, **29**, 101003.
44 H. Moustafa, C. Guizani and A. Dufresne, *J. Appl. Polym. Sci.*, 2017, **134**, 44498.
45 Y. Kim, S. Kwon and S. i. Park, *J. Appl. Polym. Sci.*, 2024, **141**, e55943.
46 A. Gowman, T. Wang, A. Rodriguez-Uribe, A. K. Mohanty and M. Misra, *ACS Omega*, 2018, **3**, 15205.
47 T. Miyata and T. Masuko, *Polymer*, 1998, **39**, 1399.
48 L. F. Ballesteros, J. A. Teixeira and S. I. Mussatto, *Food Bioprocess Technol.*, 2014, **7**, 3493.
49 A. Alghooneh, A. M. Amini, F. Behrouzian and S. M. A. Razavi, *Int. J. Food Prop.*, 2017, **20**, 2830.
50 M. J. P. A. Batista, A. F. Ávila, A. S. Franca and L. S. Oliveira, *Carbohydr. Polym.*, 2020, **233**, 115851.
51 R. C. Sun and X. F. Sun, *Carbohydr. Polym.*, 2002, **49**, 415.
52 D. N. Raba, M.-A. Poiana, A. B. Borozan, M. Stef, F. Radu and M.-V. Popa, *PLoS One*, 2015, **10**, e0138080.
53 C.-H. Dang, T.-D. Nguyen, C.-H. Dang and T.-D. Nguyen, *Waste Biomass Valorization*, 2018, **10**, 2703.
54 N. Vlachos, Y. Skopelitis, M. Psaroudaki, V. Konstantinidou, A. Chatzilazarou and E. Tegou, *Anal. Chim. Acta*, 2006, **573**, 459.
55 D. A. Mota, J. C. B. Santos, D. Faria, Á. S. Lima, L. C. Krause, C. M. F. Soares and S. Ferreira-Dias, *Processes*, 2020, **8**, 1542.
56 M. Lauberts, I. Mierina, M. Pals, M. A. A. Latheef and A. Shishkin, *Plants*, 2023, **12**, 30.
57 X. Fu, J. Su, L. Hou, P. Zhu, Y. Hou, K. Zhang, H. Li, X. Liu, C. Jia and J. Xu, *Adv. Compos. Hybrid Mater.*, 2021, **4**, 685.
58 K. Suri, B. Singh, A. Kaur, M. P. Yadav and N. Singh, *Food Chem.*, 2019, **295**, 537.
59 H. Lin, S. R. Bean, M. Tilley, K. H. S. Peiris and D. Brabec, *Food Anal. Methods*, 2020, **14**, 268.
60 C. Cao, Z. Yang, L. Han, X. Jiang and G. Ji, *Cellulose*, 2014, **22**, 139.
61 R. H. Marchessault and R. H. Marchessault, *Pure Appl. Chem.*, 1962, **5**, 107.
62 J. S. Stevanic, L. Salmén, J. S. Stevanic and L. Salmén, *Holzforschung*, 2009, **63**, 497.
63 M. Kačuráková, P. Capek, V. Sasinková, N. Wellner and A. Ebringerová, *Carbohydr. Polym.*, 2000, **43**, 195.
64 X. Liu, C. M. G. C. Renard, S. Bureau and C. L. Bourvellec, *Carbohydr. Polym.*, 2021, **262**, 117935.
65 N. Liang, X. Lu, Y. Hu and D. D. Kitts, *J. Agric. Food Chem.*, 2016, **64**, 681.
66 Y. F. Barrios-Rodriguez, Y. Devia-Rodriguez and N. G. Guzmán, *Coffee Science*, 2022, **17**, e171970.
67 E. Sermyagina, C. L. M. Martinez, M. Nikku and E. Vakkilainen, *Biomass Bioenergy*, 2021, **150**, 106141.
68 G. Rouin, M. Abdelmouleh, A. Mallah and M. Masmoudi, *Coatings*, 2023, **13**, 1745.
69 M. Barbanera and I. F. Muguerza, *Fuel*, 2020, **262**, 116493.
70 K. L. Iroba, O.-D. Baik and L. G. Tabil, *Biomass Bioenergy*, 2017, **106**, 8.
71 M. Alharbi, R. D. Bairwan, W. Y. Rizg, H. P. S. A. Khalil, S. S. A. Murshid, A. M. Sindi, M. Alissa, N. I. Saharudin and C. K. Abdullah, *Polym. Compos.*, 2024, **45**, 9317.
72 X. Zhai, J. Han, L. Chang, F. Zhao, R. Zhang, W. Wang and H. Hou, *Int. J. Biol. Macromol.*, 2024, **277**, 134505.